Dispersion Relation for Continental Shelf Waves When the Shallow Shelf Part Has an Arbitrary Width: Application to the Shelf West of Norway

MAGNUS DRIVDAL

Norwegian Meteorological Institute, Oslo, Norway

JAN ERIK H. WEBER

Department of Geosciences, University of Oslo, Oslo, Norway

JENS BOLDINGH DEBERNARD

Norwegian Meteorological Institute, Oslo, Norway

(Manuscript received 31 January 2015, in final form 6 November 2015)

ABSTRACT

The dispersion relation for continental shelf waves (CSWs) in a shelf region with an unbounded flat outer ocean, a convex-upward exponential shelf, and an interior flat region of arbitrary width D is derived. The calculations allow for a nonzero divergence of the wave motion. Some consequences of these findings are discussed for the shelf west of Norway, where the shelf at mid-Norway is quite wide, while at Lofoten it is much narrower. Furthermore, north of Lofoten, along the opening to the Barents Sea, the shelf becomes extremely wide. In this region the conditions are nearly met for a double Kelvin wave. The paper discusses how CSWs generated along the common storm track outside southwest Norway modify as they travel along the shelf. The analytical results are compared with results from a numerical barotropic ocean model with realistic shelf topography.

1. Introduction

The continental shelf can act as a waveguide for the propagation of subinertial fluctuations of sea level and currents (e.g., Allen 1980; Mysak 1980; Brink 1991). Basically, these oscillations arise as a consequence of the conservation of potential vorticity, and the phase always propagates with the coast to the right (left) on the Northern (Southern) Hemisphere (Longuet-Higgins 1965). This type of wave has been documented in several parts of the world's oceans since the 1960s (Hamon 1962), and as a general term they are often referred to as coastal trapped waves (CTWs). Examples of recent observations include the west coast of South America (Camayo and Campos 2006), along the east coast of North America (Schulz et al. 2012; Chen et al. 2014), and around Australia (Woodham et al. 2013). Continental shelf waves (CSW) can be considered to define CTWs in the case of a purely barotropic ocean (Wilkin 1988), and although the presence of stratification often plays a significant role, barotropic CSW theory has been useful in explaining observed low-frequency signals propagating along a number of continental margins. In general, stratification is expected to increase the frequency of the waves (e.g., Huthnance 1978; Brink 2006; Sansón 2012).

As well as being an important constituent of the shelf dynamics (e.g., Huthnance 1995), the presence of CSWs may affect coastal ecosystems through enhanced upwelling (e.g., Middleton and Bye 2007; Echevin et al. 2014). Furthermore the results from Weber and Drivdal (2012) indicate that these waves can induce a significant Lagrangian drift that could be relevant for the transport of, for example, biological particulate matter or pollution along the coast.

The propagation of shelf waves has been studied extensively. As discussed by Huthnance (1975) and later by, for example, Sansón (2012), there is no universal

Denotes Open Access content.

Corresponding author address: Magnus Drivdal, Norwegian Meteorological Institute, PB 43 Blindern, N-0313 Oslo, Norway.
E-mail: magnus.drivdal@met.no

DOI: 10.1175/JPO-D-15-0023.1

dispersion relation for waves over arbitrary topography, but exact analytical solutions can be found for idealized shelf shapes. Some of these include solutions for a linearly varying (Pedlosky 1982), exponential concave-upward (Ball 1967) and exponential convex-upward (Buchwald and Adams 1968) shelf slope profile. More recently, Schulz et al. (2012) combined the solutions of Pedlosky (1982) and Ball (1967) to develop a dispersion relation for CSWs in the Mid-Atlantic Bight. Although dispersion relations can be found numerically for arbitrary bathymetry in the cross-shelf direction (e.g., Brink and Chapman 1985; Gjevik 2002; Kaoullas and Johnson 2010), the analytical solutions can be useful for analyzing observational data and for comparing wave propagation characteristics on one portion of the shelf to another (e.g., Camayo and Campos 2006; Schulz et al. 2012).

Barotropic models have on several occasions been used to study the effect of an abrupt change in the shelf width (e.g., Huthnance 1987; Webster 1987; Wilkin and Chapman 1987; Yankovsky and Chapman 1995). For the Australian shelf, Woodham et al. (2013) find from observations that the sea surface height amplitude and the phase speed of CTWs are closely correlated with the shelf width. Schulz et al. (2012) also find a strong dependency of phase speed on shelf width using their analytical model for a concave-upward shelf slope representative of the Mid-Atlantic Bight. Here we will focus on a convex-upward shelf slope that can be suitable in other areas, such as parts of the Australian shelf (Buchwald and Adams 1968), the western coast of South America (Camayo and Campos 2006), and the western coast of Norway (Weber and Drivdal 2012).

In this study we adapt the model of Buchwald and Adams (1968), who considered freely propagating shelf waves over 1) a coastal bounded shelf with exponentially increasing depth seaward and 2) a shelf with the same depth profile, but without a coastal boundary. These authors refer to the latter case of an infinitely wide shelf as an "interior shelf." This configuration is a special case of that supporting double Kelvin waves (see Longuet-Higgins 1968). Defining a flat shelf area of arbitrary width shoreward of the shelf slope, we develop a more general dispersion relation. The dispersion relation is valid for any shelf width, which increases the applicability of the theory to shelf configurations found in the ocean. Some of the implications of this model are discussed, and applications to the Norwegian shelf are presented. Finally, the analytical model is compared with results from a numerical barotropic ocean model. The effect of stratification can be quantified in terms of the Burger number $\mathrm{Bu} = [NH/(fL)]^2$; see Huthnance (1978), where L is a typical horizontal length scale and N is the Brunt-Väisälä frequency. Taking $L \sim 150$ km, which is a representative value for the width of the sloping shelf west of Norway, we find from Slørdal et al. (1994) that $\mathrm{Bu} \sim 0.1$. This indicates that the effect of stratification on CSWs is small in this region.

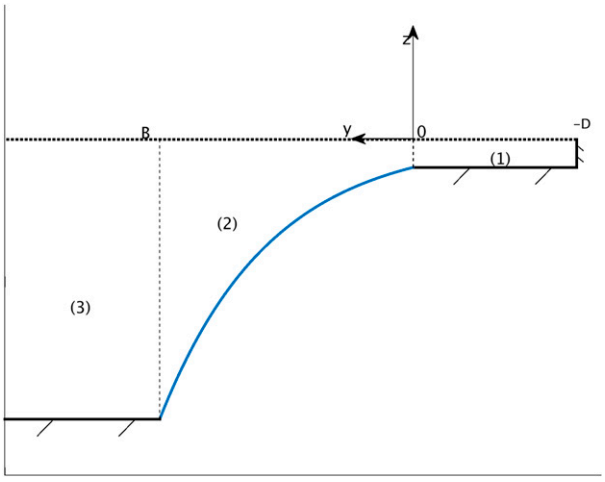

FIG. 1. Shelf model: the shelf in area 1 is bounded by land at $y = -D$, has a constant depth H_1, and reaches the shelf break at $y = 0$. The depth of the continental slope (area 2) increases exponentially as $H_2 = H_1 \exp(2by)$ until $y = B$. The deep ocean (area 3) of constant depth $H_3 = H_1 \exp(2bB)$ extends to infinity.

2. Linear theory

The continental shelf wave problem is solved along the lines of Buchwald and Adams (1968) and Gill and Schumann (1974; see also Gill 1982). We here disregard the effect of bottom friction. The linearized equations for the barotropic part of the CSW field are

$$U_t - fV = -gH\eta_x, \tag{1a}$$

$$V_t + fU = -gH\eta_y, \quad \text{and} \tag{1b}$$

$$\eta_t = -U_x - V_y, \tag{1c}$$

where t denotes time and x and y are the alongshore and cross-shore horizontal axes, respectively. The corresponding velocity components are (u, v), and η is the surface elevation. Furthermore, f is the constant Coriolis parameter, and g is the acceleration due to gravity. The fluxes (U, V) are defined by

$$(U, V) = \int_{-H}^{0} (u, v)\, dz. \tag{2}$$

The bottom profile is given by (see Fig. 1)

$$H = \begin{cases} H_1, & -D \le y \le 0 \\ H_2 = H_1 e^{2by}, & 0 \le y \le B \\ H_3 = H_1 e^{2bB}, & y \ge B. \end{cases} \tag{3}$$

Here D is the width of the interior shelf region denoted by 1 in Fig. 1, where the depth is constant and equal to H_1. Furthermore, B characterizes the width of the depth-varying shelf region 2, and the deep ocean (region 3) has constant depth $H_3 = H_1 \exp(2bB)$, where b is a constant that yields the depth variation in region 2. The deep ocean extends to infinity in the y direction.

The set of Eq. (1) can be combined into one equation for the surface elevation η. Taking ∂[Eq. (1a)]/$\partial t + f$[Eq. (1b)], $-f$[Eq. (1a)] + ∂[Eq. (1b)]/∂t, and $(\partial^2/\partial t^2 + f^2)$[Eq. (1c)], Eqs. (1a)–(1c) become

$$\left(\frac{\partial^2}{\partial t^2} + f^2\right) U = -gH\eta_{xt} - gfH\eta_y, \tag{4a}$$

$$\left(\frac{\partial^2}{\partial t^2} + f^2\right) V = -gH\eta_{yt} + gfH\eta_x, \quad \text{and} \tag{4b}$$

$$\left(\frac{\partial^2}{\partial t^2} + f^2\right) \eta_t = -\left(\frac{\partial^2}{\partial t^2} + f^2\right)(U_x + V_y). \tag{4c}$$

Taking ∂[Eq. (4a)]/$\partial x + \partial$[Eq. (4b)]/∂y and using Eq. (4c), we arrive at

$$\frac{\partial}{\partial t}\left[\frac{\partial}{\partial x}\left(H\frac{\partial \eta}{\partial x}\right) + \frac{\partial}{\partial y}\left(H\frac{\partial \eta}{\partial y}\right) - \frac{1}{g}\left(\frac{\partial^2}{\partial t^2} + f^2\right)\eta\right] = f\frac{dH}{dy}\frac{\partial \eta}{\partial x}. \tag{5}$$

We here consider low-frequency (subinertial) waves. If $\eta \sim \exp[i(kx - \omega t)]$, where k and ω are the wavenumber and the frequency, respectively, this means that $|\omega| < f$. Under certain circumstances this problem can be simplified by using the rigid-lid approximation (e.g., Buchwald and Adams 1968; Smith 1972; Gill and Schumann 1974). However, this may lead to spurious results for small wavenumbers when the shallow inner shelf becomes very wide (Longuet-Higgins 1968). We intend to investigate the dispersion relation for an arbitrary width D of the inner shelf, allowing for a freely moving surface. With $\eta = \eta(y)\exp[i(kx - \omega t)]$, Eq. (5) reduces to

$$\frac{d}{dy}\left(H\frac{d\eta}{dy}\right) - \left(Hk^2 + \frac{f^2 - \omega^2}{g} - \frac{kf}{\omega}\frac{dH}{dy}\right)\eta = 0. \tag{6}$$

Now, using the transform $\eta(y) = H^{-1/2}s(y)$, Eq. (6) becomes

$$\frac{d^2 s}{dy^2} + \left(-k^2 - b^2 + \frac{2kbf}{\omega} - \frac{f^2 - \omega^2}{gH}\right)s = 0. \tag{7}$$

We here assume that $\omega^2 \ll f^2 + gHk^2$. This assumption filters out Poincaré waves (nontrapped waves) from the flat parts of our model domain. In the flat-bottomed regions the solutions become

$$\begin{aligned} s_1 &= A_1 \exp(\kappa_1 y) + C_1 \exp(-\kappa_1 y), \quad y \le 0, \\ s_3 &= C_3 \exp(-\kappa_3 y), \quad y \ge B, \end{aligned} \tag{8}$$

where

$$\begin{aligned} \kappa_1 &= (k^2 + \delta_1^2)^{1/2}, \quad \delta_1 = \frac{f}{(gH_1)^{1/2}}, \\ \kappa_3 &= (k^2 + \delta_3^2)^{1/2}, \quad \delta_3 = \frac{f}{(gH_3)^{1/2}}. \end{aligned} \tag{9}$$

Over the sloping bottom we simplify Eq. (7). Realizing that the bottom gradient resides in the $2kbf/\omega$ term, we approximate the depth in the last term by the mean depth, that is, we take $H \approx H_m = (H_1 + H_3)/2$. This approximation will be discussed in the next section. Hence, we may write

$$s_2 = C_2 \sin(ly) + D_2 \cos(ly), \quad 0 \le y \le B, \tag{10}$$

where l, for certain wavenumbers k, may be purely imaginary. For Eq. (10) to be a solution of Eq. (7), we must have

$$l^2 = 2kbf/\omega - k^2 - b^2 - \delta_m^2, \tag{11}$$

where

$$\delta_m = \frac{f}{(gH_m)^{1/2}}. \tag{12}$$

To obtain $l = l(k)$ for the given geometry, we must apply the boundary conditions. These are the continuity of sea level and volume fluxes in the y direction at $y = 0$ and at $y = B$, as well as zero normal flux at $y = -D$. To express the normal flux boundary conditions in terms of the amplitude function s, we consider Eq. (4b) with $V = V(y)\exp[i(kx - \omega t)]$ and $\eta = H^{-1/2}s(y)\exp[i(kx - \omega t)]$:

$$\frac{i(f^2 - \omega^2)V}{\omega g H^{1/2}} = -\left(\frac{kf}{\omega} - b\right)s - \frac{ds}{dy}. \tag{13}$$

In terms of s, the boundary conditions then become

$$\frac{ds_1}{dy} + \frac{kf}{\omega}s_1 = 0, \quad y = -D; \tag{14a}$$

$$s_1 = s_2, \quad y = 0; \tag{14b}$$

$$\frac{ds_1}{dy} = \frac{ds_2}{dy} - bs_2, \quad y = 0; \tag{14c}$$

$$s_2 = s_3, \quad y = B; \quad \text{and} \tag{14d}$$

$$\frac{ds_3}{dy} = \frac{ds_2}{dy} - bs_2, \quad y = B. \tag{14e}$$

Inserting Eqs. (8) and (10) into Eq. (14), it is found that

$$\tan lB = \frac{l(R\kappa_1 + \kappa_3)}{b^2 + l^2 + b(R\kappa_1 - \kappa_3) - R\kappa_1\kappa_3}, \quad (15)$$

where κ_1 and κ_3 are defined in Eq. (9) and R is given by

$$R = \frac{kf - \omega\kappa_1 + (kf + \omega\kappa_1)\exp(-2\kappa_1 D)}{kf - \omega\kappa_1 - (kf + \omega\kappa_1)\exp(-2\kappa_1 D)}. \quad (16)$$

Equation (15) for l is general. For the special case of no inner shelf ($D = 0$), we are back to the problem first treated by Buchwald and Adams (1968). They applied the rigid-lid approximation, that is, $\delta_1 = \delta_m = \delta_3 = 0$. Then Eq. (15) reduces to

$$\tan(lB) = -\frac{l}{k + b}, \quad (17)$$

as in Buchwald and Adams (1968). For a very wide inner shelf ($D \to \infty$), this problem becomes a special case of the double Kelvin wave problem with continuous depth profile solved by Longuet-Higgins (1968). In that case $R \to 1$ in Eq. (15), which then reduces to

$$\tan(lB) = \frac{l(\kappa_1 + \kappa_3)}{b^2 + l^2 + b(\kappa_1 - \kappa_3) - \kappa_1\kappa_3}. \quad (18)$$

Furthermore, in the rigid-lid case ($\delta_1 = \delta_m = \delta_3 = 0$), we find

$$\tan(lB) = \frac{2kl}{b^2 + l^2 - k^2}, \quad (19)$$

which is Buchwald and Adams's (1968) result for an infinitely wide shelf. As first pointed out by Longuet-Higgins (1968), the rigid-lid assumption in this case leads to erroneous results when $k \to 0$ (yielding nonzero frequency and negative group velocity).

Rearranging Eq. (11), the dispersion relation for continental shelf waves with this bottom topography becomes

$$\frac{\omega}{f} = \frac{2kb}{k^2 + l^2 + b^2 + \delta_m^2}. \quad (20)$$

In the following section, we solve the CSW problem with a freely moving surface for selected sections of the Norwegian continental shelf. Since the rigid-lid approximation is so frequently used for this problem (Buchwald and Adams 1968; Smith 1972; Gill and Schumann 1974), we compare our results for a free-surface calculation with those obtained applying a rigid lid at the surface.

3. Application to the Norwegian shelf

As can be seen in Fig. 2, the Norwegian continental shelf is highly irregular, with varying width in the direction normal to the coastline. The shelf extends from the north of the mainland into the Barents Sea toward the Svalbard archipelago. We aim to investigate if the simple analytical model for CSWs over an exponentially varying depth described in the previous section can give an indication to whether a disturbance generated over the shelf southwest of Lofoten (see Fig. 2) can propagate as a shelf wave over the varying topography along the coast and farther along the edge toward Svalbard. With appropriate values of H_1, H_3, B, and D, the relation from Eq. (3) determines the values of H_2 and b and can be used to construct a model of the cross-shelf bottom topography. A comparison between this idealized bottom topography profile with the bottom topography from the numerical model presented in section 5 (along the transect shown as a red line in Fig. 2) can be seen in Fig. 3. The wider shelf sections both southwest and north of Lofoten are very irregular, but representative mean values for the shelf configuration are given in Table 1. It can be seen from Fig. 2 that the southwestern shelf is bounded by the west Norwegian coastline, while the shallow region east of the escarpment north of Norway stretches far into the Barents Sea. The nearest land that bounds this region is the island of Novaya

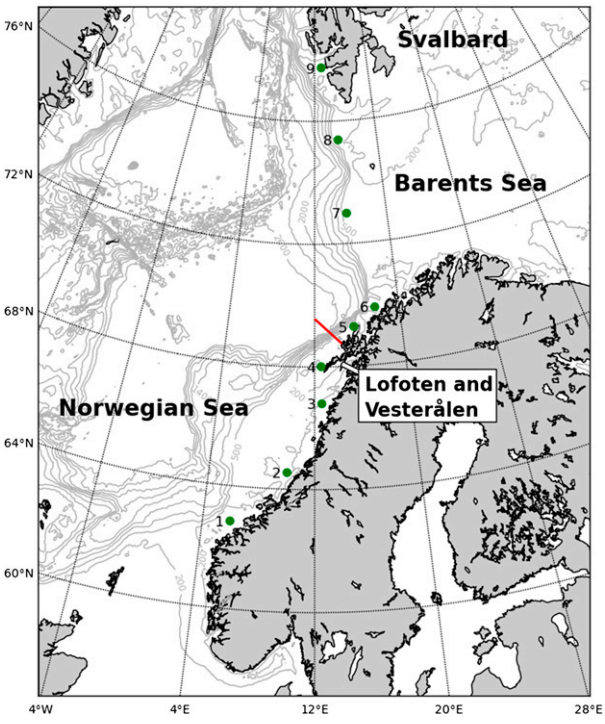

FIG. 2. Map of the Norwegian coastal area with bottom contours. The narrow continental shelf outside Lofoten and Vesterålen is bordered by a wider shelf both to the north and southwest. Green points indicate locations where time series of SSH are taken (these will subsequently be referred to as points 1–9, counting from south to north). The bottom topography is from the numerical model described in section 5.

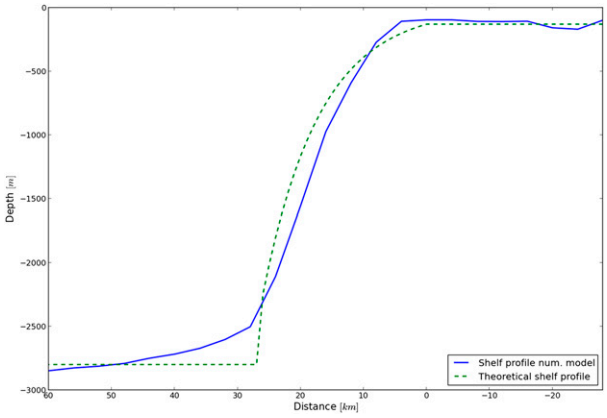

FIG. 3. Cross-shelf bottom topography outside Lofoten. The blue solid line is the bottom topography from the numerical model described in section 5, corresponding to the section indicated by the red line in Fig. 2, while the green dashed line is the model shelf using Eq. (3) with the values in Table 1.

Zemlya, approximately 1200 km to the east (not seen in Fig. 2). For the shelf southwest of Lofoten, we consider a width of 155 km to be representative, which is similar to that used by Martinsen et al. (1979). With these values for the bottom profiles, the dispersion relations for the first and second modes for all three shelf sections can be calculated from Eq. (20) and Eq. (15), and the result is shown in Fig. 4. Since strong wind events historically occur at the southwestern part of the Norwegian shelf (apart from polar lows), before moving northeast and inland, it is natural to consider this part of the shelf as the generation area for CSWs. Typical periods here will be 1–3 days; see Gjevik (2000). From Fig. 4 we realize that any first-mode CSW to pass the Lofoten region must have a frequency less than $0.74f$ (maximum of the green curve). At mid-Norway this frequency corresponds to a wave with wavelength of about 680 km (blue curve). Obviously, all first-mode CSWs with wavelengths longer than this can pass into the Lofoten area. However, conserving frequency, the local wavelength here will be much shorter, which also means a much lower phase speed and lower group velocity. This may lead to CSW breaking in the region outside Lofoten and thereby to the enhancement of the quite strong current in this region. From Gascard et al. (2004) we observe that the water mass over the shallow shelf is low-salinity Norwegian Coastal Current (NCC) water, extending outwards to about 60 km from the coast. From the estimated flux of 0.7 Sverdrups (Sv; $1\,\text{Sv} \equiv 10^6\,\text{m}^3\,\text{s}^{-1}$) for the NCC (Björk et al. 2001), this yields mean velocities of about $0.2\,\text{m}\,\text{s}^{-1}$. The waves that leave Lofoten will continue with a much longer wavelength in the Barents Sea opening, as can be seen from the red solid curve in Fig. 4. However, if the wave periods are long ($\omega/f \lesssim 0.22$), the wave energy may travel past Lofoten and in the Barents Sea as second-mode CSWs (red dashed line). We also note from Fig. 4 that the maximum frequencies in the approach region (south of Lofoten) and outside Lofoten (blue and green curves) are slightly greater than in the Barents Sea opening (red curve). In principle, this means that waves of a very limited frequency range may not propagate into the Barents Sea. In practice, however, since the difference in maximum frequency is so small, we expect most waves of frequencies lower than the maximum frequency south of Lofoten to be able to pass into the Lofoten area and continue into the Barents Sea.

TABLE 1. Parameters for the model cross-shelf bathymetry.

	H_1	H_3	B	D
Southwest of Lofoten	200 m	3200 m	10 km	155 km
Lofoten and Vesterålen	130 m	2800 m	28 km	28 km
North of Lofoten	300 m	2800 m	100 km	1200 km

We note from Fig. 4 that our maximum frequency ω is close to $0.7f$. We have previously assumed that $\omega^2/f^2 \ll 1 + gHk^2/f^2$ in Eq. (7) to ensure trapped waves. Inserting typical values ($H \sim 300\,\text{m}$, $k \sim 5 \times 10^{-6}\,\text{m}^{-1}$), the requirement for this case becomes $\omega^2/f^2 \ll 6$, so the result $\omega/f \sim 0.7$ is well within this limit.

As mentioned before, the rigid-lid approximation leads to spurious results for small wavenumbers when the inner shelf is very wide. To see how finite shelves are affected, we have calculated the dispersion curves for the first mode at our three previous locations at the Norwegian shelf, using the rigid-lid approximation.

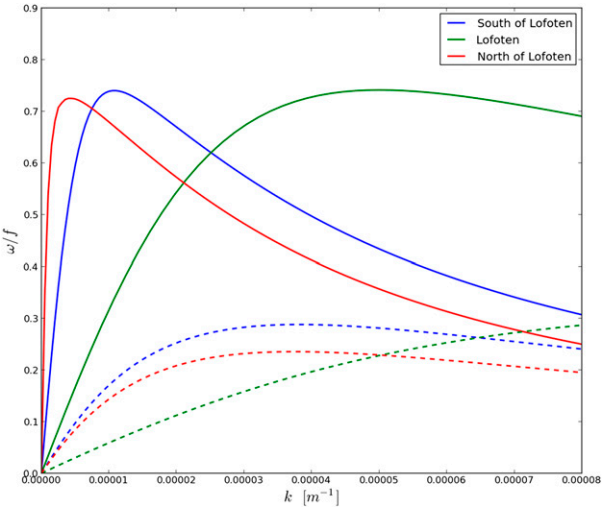

FIG. 4. Dispersion relations for the cross-shelf profiles corresponding to the sections south of Lofoten (blue lines), seawards of Lofoten (green lines), and north of Lofoten (red lines). First modes are displayed as solid lines, while second modes are dashed lines.

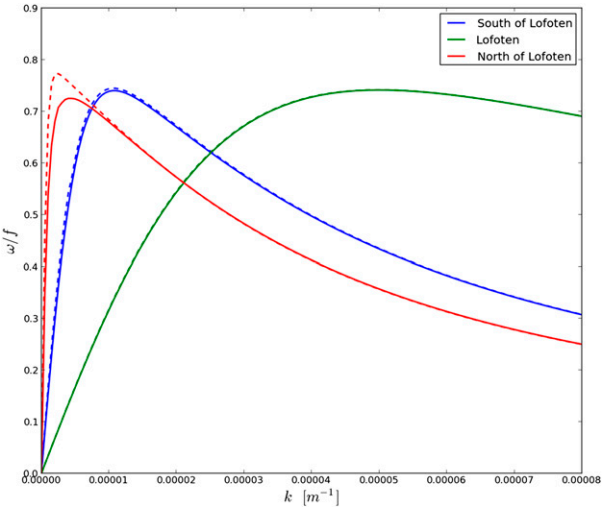

FIG. 5. As in Fig. 4, but where the dashed lines are the first modes calculated from the rigid lid approximation.

The results are plotted in Fig. 5. We find noticeable differences only in the Barents Sea opening ($D/B = 12$); see Table 1. Here we have a deviation at the peak frequency of about 8%. All in all, it must be concluded that the rigid-lid approximation works quite well along the shelf outside Norway. In this connection it is also relevant to consider the approximation $H_m = (H_1 + H_3)/2$ in the dispersion relation [Eq. (20)]. We realize that this term is related to the divergence effect. Whether we use the extreme values $H_m = H_1$ or $H_m = H_3$ is not crucial, since the divergence effect plays a minor role along the Norwegian shelf, as demonstrated by the success of the rigid-lid approximation (see, e.g., Fig. 5). In our case $H_m = (H_1 + H_3)/2$ appears to yield a reasonable middle-of-the-road value.

4. Cross-shelf variation

As first reported by Buchwald and Adams (1968) for an infinite inner shelf, the offshore variation (the y variation) of the CSW field over the slope was hyperbolic for small k, that is, the wavenumber l was purely imaginary. On the other hand, for vanishing inner shelf ($D = 0$), l is always real, so the wave field varies sinusoidally over the slope. We investigate this problem for arbitrary shelf width, and apparently there must be a threshold value of D that marks this transition. Since the rigid lid works well for small and moderate D in our case, we use it to simplify the calculations, that is, we take $\delta_1 = \delta_m = \delta_3 = 0$ in Eqs. (20) and (15). Scaling with B, we now may define the dimensionless quantities

$$\hat{k} = kB, \quad \hat{l} = lB, \quad \hat{a} = \frac{D}{B}, \quad \hat{\sigma} = \frac{\omega}{f}, \quad \hat{b} = bB. \tag{21}$$

Then, from Eqs. (20) and (15),

$$\hat{\sigma} = \frac{2\hat{k}\hat{b}}{\hat{b}^2 + \hat{k}^2 + \hat{l}^2} \tag{22}$$

and

$$\tan(\hat{l}) = \frac{(1+T)\hat{k}\hat{l}}{T\hat{l}^2 - (\hat{k} - \hat{b}T)(\hat{k} + \hat{b})}, \tag{23}$$

where now

$$T = \tanh(\hat{a}\hat{k}). \tag{24}$$

Similar to the analysis of Buchwald and Adams (1968) for the special case of an interior shelf, the denominator on the right-hand side (RHS) of Eq. (23) has zeros. Since we now consider a finite shelf width D, we realize that $0 < T < 1$, and since by definition $\hat{k}, \hat{b} > 0$, it can be seen from Eq. (23) that zeros now have to occur for $\hat{k}^2 < \hat{l}^2 + \hat{b}^2$. Let G be the graph of the RHS of Eq. (23). When $\hat{l}$ is real, G tends to infinity at $\hat{l} = \delta$, where

$$\delta^2 = \frac{\hat{k}^2 + \hat{k}\hat{b} - \hat{k}\hat{b}T}{T} - \hat{b}^2. \tag{25}$$

It should be noted that compared to the interior shelf considered by Buchwald and Adams (1968), the asymptotic value occurs for larger $\hat{l}$. This is because δ becomes larger for smaller values of $\hat{a}$. In practice T rapidly increases toward 1 as $\hat{a}$ increases. The graphical solutions of Eq. (23) for $\hat{k} > \hat{b}T$ can be seen in Fig. 6 (bottom panel). It can be seen that for $\hat{k} \geq \hat{b}T$, there is only one solution of Eq. (23) in each interval $(n-1)\pi < \hat{l} < n\pi$, where $n = 1, 2, 3$, etc. Also observe that for $\hat{k} = \hat{b}T$, that is, $\delta = 0$, all intersections are at $\hat{l} < (n - 1/2)\pi$. The case of $\hat{k} < \hat{b}T$ has been sketched in Fig. 6 (top panel). Combining the two cases, it may be seen that for $n \geq 2$, $\hat{l}_n(\hat{k})$ varies monotonically from $(n-1)\pi$ to $n\pi$ as $\hat{k}$ varies from 0 to ∞. This is very similar to the result of Buchwald and Adams (1968) for the interior shelf. As seen in Fig. 6 (top panel), Eq. (23) has no roots in the interval $0 < \hat{l} < \pi$ for $\hat{k} < \hat{k}_0$, where $\hat{k}_0 > 0$ is the minimum value of $\hat{k}$ for real $\hat{l}$ that occurs in the limit $\hat{l} \to 0$. From the third-order Taylor expansion of Eq. (23) about $\hat{l} = 0$ and dividing by $\hat{l}$, it is found that

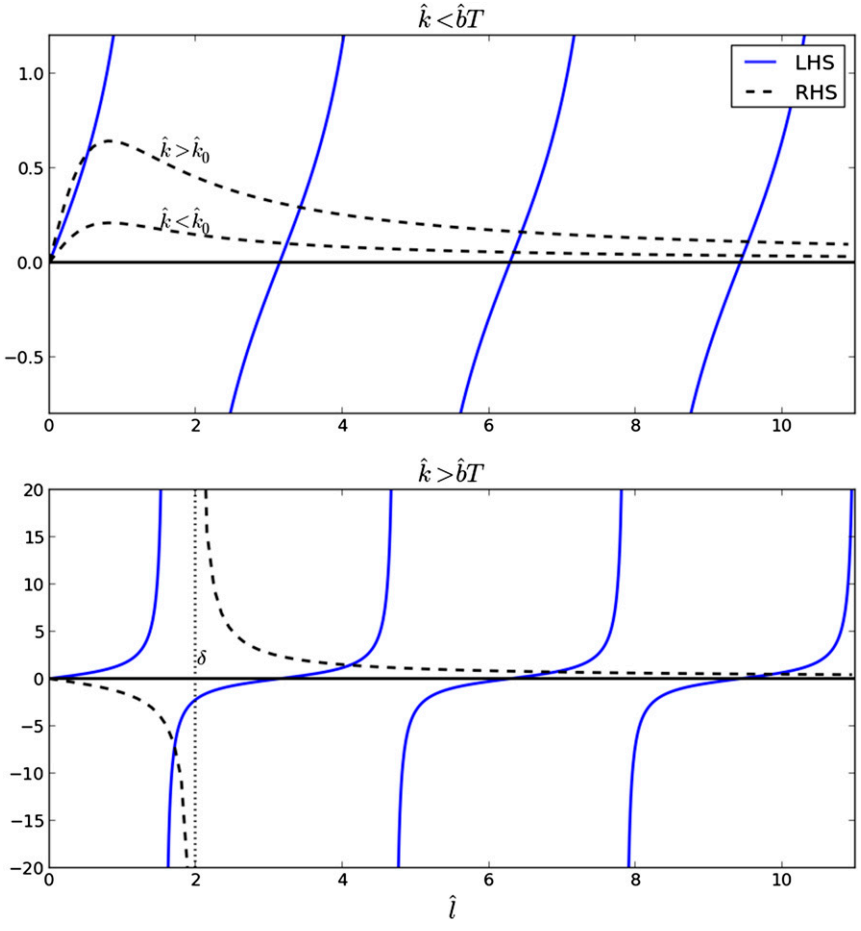

FIG. 6. Graphical solutions of Eq. (23) for (top) $\hat{k} < \hat{b}T$ and (bottom) $\hat{k} > \hat{b}T$. The LHS of Eq. (23) is indicated by the solid line and the RHS by the dashed line.

$$1 + \frac{1}{3}\hat{l}^2 = -\frac{(1+T)\hat{k}}{(\hat{k}-\hat{b}T)(\hat{k}+\hat{b})} + \frac{(1+T)\hat{k}T}{(\hat{k}-T\hat{b})^2(\hat{k}+\hat{b})^2}\hat{l}^2. \tag{26}$$

With $\hat{k} = \hat{k}_0$, $T = T_0 = \tanh(\hat{k}_0\hat{a})$, and neglecting terms of order $\hat{l}^2$, this reduces to

$$\tanh(\hat{k}_0\hat{a}) = \frac{\hat{k}_0^2 + (1+\hat{b})\hat{k}_0}{\hat{b}^2 + (\hat{b}-1)\hat{k}_0}. \tag{27}$$

From Eq. (27) it can be seen that the value of $\hat{k}_0$ depends on the value of $\hat{a}$. In the limits of an interior shelf ($\hat{a} \to \infty$, $T_0 = 1$) and an exponential shelf ($\hat{a} \to 0$, $T_0 = 0$), the solutions of Eq. (27) become $\hat{k}_0 = \sqrt{1+\hat{b}^2} - 1$ and $\hat{k}_0 = 0$, respectively (Buchwald and Adams 1968). The solution for intermediate values of $\hat{a}$ can be visualized by plotting the left-hand side (LHS) and RHS of Eq. (27), as shown in Fig. 7. As can be seen in Fig. 7, Eq. (27) has no roots for values of $\hat{a}$ below some threshold value $\hat{a}_t$. The value of $\hat{a}_t$ can be found by considering the limit of Eq. (27) as $\hat{k}_0 \to 0$. From Fig. 7 it can be seen that for a solution to exist, the LHS must be larger than the RHS in this limit. In terms of Eq. (27), using a second-order Taylor expansion, this means that

$$\hat{a} > \frac{1+\hat{b}}{\hat{b}^2} = \hat{a}_t. \tag{28}$$

Accordingly, for $\hat{a} > \hat{a}_t$, Eq. (27) can be solved to find the value of $\hat{k}_0$. For values of $\hat{k} < \hat{k}_0$, $\hat{l}$ is then purely imaginary. For values of $\hat{a} \le \hat{a}_t$, however, Eq. (27) has no solutions, which means that $\hat{l}$ is real for all $\hat{k}$, and the values for the first mode can be found by solving Eq. (23) (lines will always cross in Fig. 6). In dimensional terms, the threshold shelf width D_t becomes from Eq. (28)

$$D_t = \frac{1+bB}{b^2 B}. \tag{29}$$

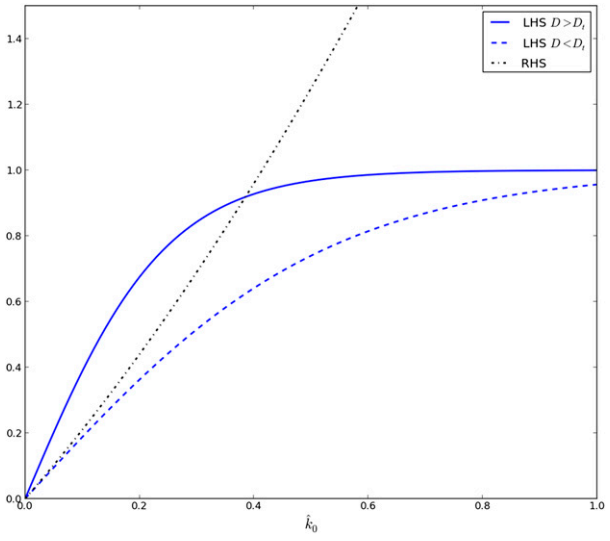

FIG. 7. Graphical solutions of Eq. (27). The left-hand side ($D > D_t$, solid line; $D < D_t$, dashed line) is denoted by LHS, and the right-hand side (dashed-dotted line) by RHS.

In the preceding sections, we have used idealized bottom topography in three different locations along the Norwegian shelf, so the results must be viewed in a qualitative sense. In the next section, we perform some numerical experiments on CSW propagation with more realistic bottom topography to see how well our idealized approach catches the real physics of the problem.

5. Numerical example

A common way to detect coastally trapped waves is to investigate their signature in the sea surface height (SSH) using data from tide-gauge observations and/or ocean circulation models (e.g., Sheng et al. 2006; Thiebaut and Vennell 2010; Schulz et al. 2012; Woodham et al. 2013; Chen et al. 2014). There are few tide-gauge stations along the west coast of Norway, and some of them are located in sheltered areas between islands and inside fjords. Furthermore, there are no measurements over the shelf between Norway and Svalbard. To investigate the propagation of CSWs along the shelf west of Norway, we have therefore applied a two-dimensional (2D) depth-averaged version of the Regional Ocean Modeling System (ROMS; e.g., Shchepetkin and McWilliams 2005; Haidvogel et al. 2008). Similar 2D models have been used operationally to forecast storm surges in several countries of Europe (e.g., Flather 2000). The present setup of ROMS covers the Nordic Seas, including the adjacent North Sea, Barents Sea, and the Baltic Sea. Grid spacing is approximately 4 km in the horizontal direction, and a polar-stereographic map projection is utilized. The bathymetry is based on the GEBCO_08 grid (version 20100927, http://www.gebco.net), which has global coverage of 30 arcs × 30 arcs resolution. This fine-resolution bathymetry is interpolated to the model grid using distance-weighted averages over the points falling within a model grid cell. The model simulates the barotropic mode, using a constant reference density. At open boundaries, we apply the free surface Chapman (1985) and 2D-momentum Flather (1976) boundary condition scheme as proposed by Marchesiello et al. (2001). Only the linearized inverse barometer effect is added at open boundaries. Bottom stress is based on a quadratic law, with respect to depth-averaged currents. External forcings are mean sea level pressure (MSLP) and surface stress, where calculation of the latter follows Charnock (1955). Wind and MSLP are extracted from the ERA-Interim reanalysis (Dee et al. 2011).

In the study by Martinsen et al. (1979), both Kelvin waves and shelf waves are found along the coast as well as propagating double Kelvin waves along the escarpment between the north of Norway and Svalbard. However, these authors use a very simple bottom topography (step shelf), and the model has a coarse resolution. In fact, from the analytical shelf wave solutions for a step shelf, it can be seen that the dispersion relation becomes equal to the dispersion relation for double Kelvin waves in the shortwave limit, which makes it hard to distinguish them from each other. Several other numerical studies have also considered CSW propagation along the Norwegian coast (e.g., Gjevik 1990, 1991; Slørdal et al. 1994). However, these rely on coarse horizontal grid resolution [Gjevik (1990, 1991) uses 50 km and Slørdal et al. (1994) use 20 km] and a simplified coastline. These simplifications make it hard to draw any conclusions to how the irregular coastline of Norway, with abrupt changes in shelf width (e.g., the narrow shelf at Lofoten), affects CSW propagation.

To isolate the sea surface response to the atmospheric forces, the model is run without tidal forcing. For this study the model is run with atmospheric forcing from a storm event that occurred in February 1989. This event is chosen as an example because the low-pressure system causing the storm was quite isolated and resulted in an unusually strong SSH signal along the coast. As the front of the storm reached the coast on 15 February at 0000 UTC, the pressure in the center was about 950 hPa, and the 10-m wind speed was approximately 26 m s^{-1}. To analyze the model results, we define an SSH anomaly (SSA) by subtracting the winter mean (January–March) from the SSH. The development of the resulting SSA for four points along the coast can be seen in Fig. 8. Clearly, there is a peak in SSA after the storm reaches the coast at all four stations shown, and it can be seen that the SSA

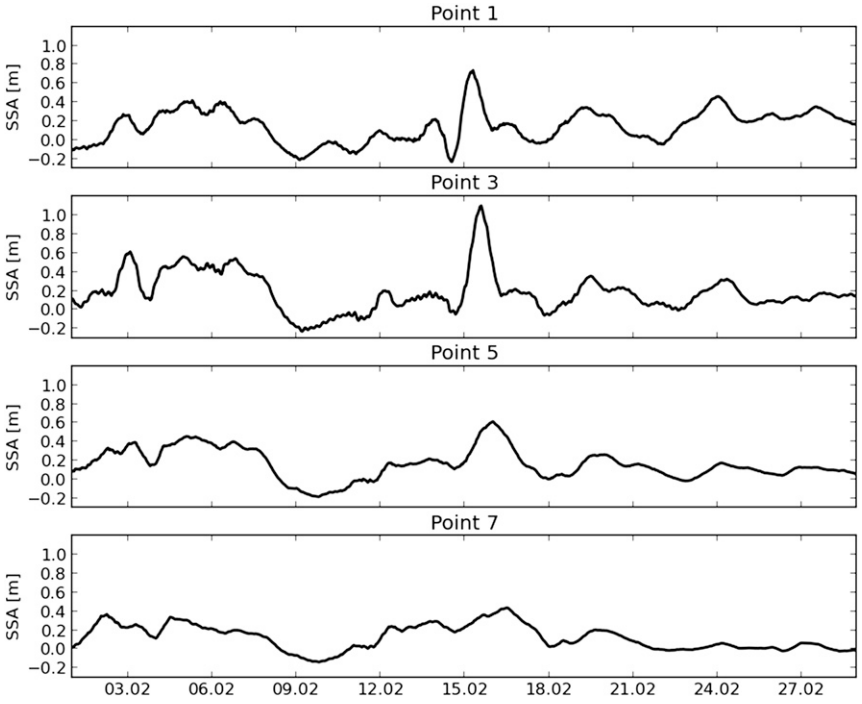

FIG. 8. Time series of SSA from the model at four points along the coasts. The points are numbered as shown in Fig. 2.

is highly correlated over the whole month, with a small time lag.

The present setup gives reasonable results for storm surges along the Norwegian coast, but it is very dependent on the quality of the atmospheric forcing. Comparing it with observations for tide-gauge stations along the coast of Norway, the present setup with ERA-Interim forcing gives correlation coefficients between observed storm surge residual (difference between observed water level and tidal predictions) and modeled SSH of around 0.96 for the period 1 January to 30 April 1989. Adjusting for differences in mean water level for the period considered, root-mean-square errors are around 0.06 m at the stations.

The modeled SSA response to the storm for the whole model domain can be seen in Fig. 9, together with the position of the storm center, indicated by circles. Typically for the storms reaching the western coast of Norway, the storm follows a path at an angle along the coast, approaching land as it travels northward. Since the storm has a direction along the coast in the same direction as the propagation of a CSW, it is not straightforward to distinguish between the specific SSH response of a CSW and the specific response to the storm itself. However, several interesting features can be seen in Fig. 9. First, we notice that the SSA signal seems to travel along the escarpment between the north of Norway and Svalbard. Second, there is a signal that seems to propagate like a coastal Kelvin wave eastward along the northern coast of Norway into the Barents Sea. To study the free wave response without atmospheric interference, the model is also run with the atmospheric forcing turned on only during the time when the storm passes the southern part of the shelf in Fig. 2. In this idealized experiment with the storm activated for a limited period, we have spun up the model to steady state based on the winter mean (1 January to 30 April) MSLP and surface stress. Then at 0600 UTC 14 February, we start a 12-h linear interpolation from the mean field to the actual synoptic forcing, with full forcing from 1800 UTC onward for 30 h until 0000 UTC 16 February. The forcing is then interpolated back to the mean forcing, and this is held constant from 1200 UTC 16 February. A Hovmöller diagram constructed from the time series of SSA from this idealized run and the distance between the points along the shelf indicated in Fig. 2 can be seen in Fig. 10. Here, a rough estimate of the propagation speed can be made from the slopes of the wave features. From Fig. 10 it can be seen that the signal is damped, and the waves die out in time as the model adjusts to the constant background forcing. There is a clear tendency for slower propagation along the narrow shelf, which can be seen as steeper slopes of the wave features at the points along

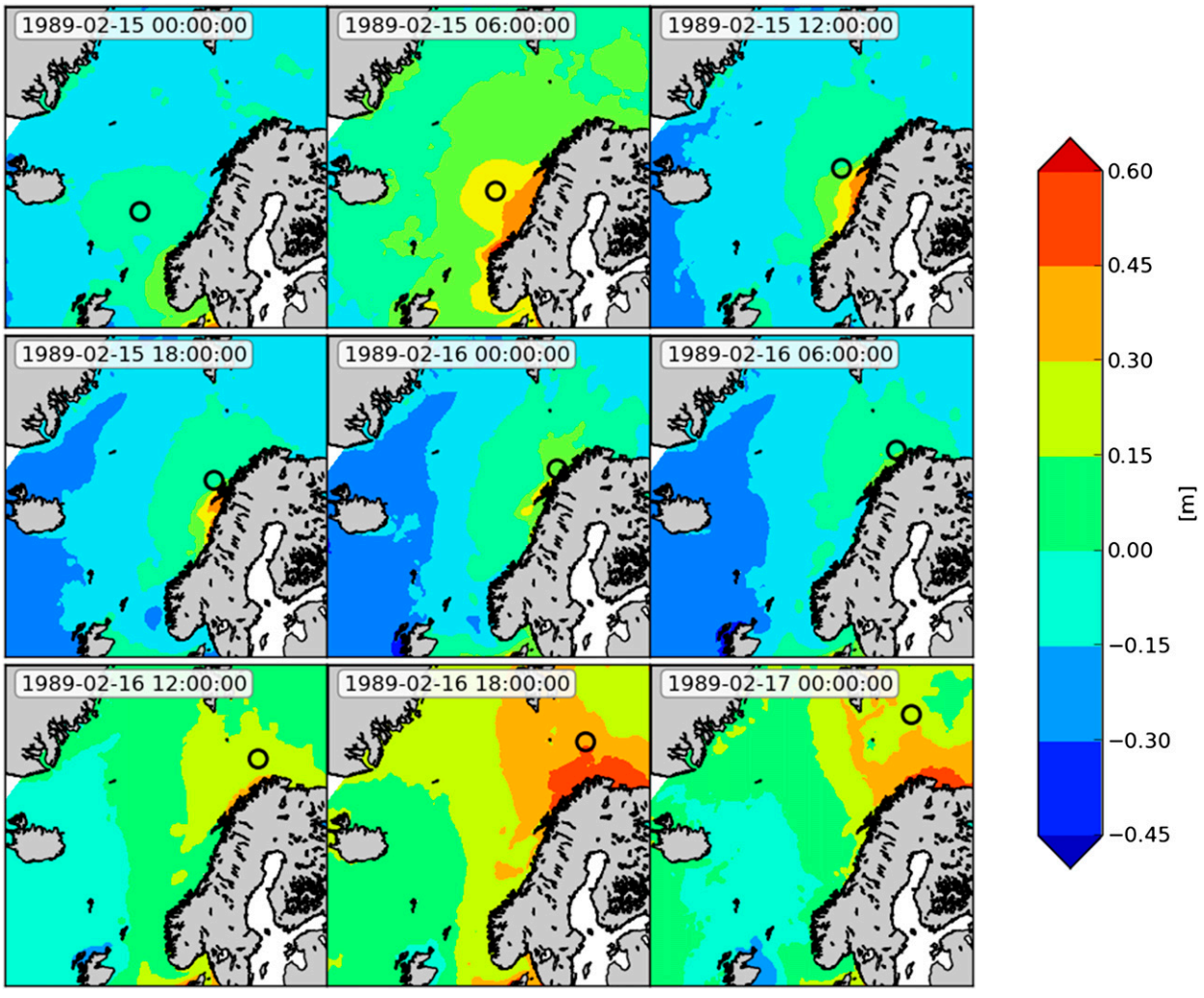

FIG. 9. SSA from the model when full atmospheric forcing is applied. The approximate position of the low-pressure center is indicated by a black circle.

Lofoten (vertical lines 3–5 from the left in Fig. 10, corresponding to points 4–6 in Fig. 2). From the slope of the feature on 18–19 February, the phase speed south of Lofoten (points 1–3) can be estimated to about 24 m s^{-1}, while it drops to approximately 5 m s^{-1} along the narrow shelf farther north (points 4–6). As the shelf widens to the north after Lofoten, the signal seems to propagate much faster, but the amplitude of the signal becomes so low that it is hard to give an estimate of the exact phase speed in this region from the Hovmöller diagram. From the mean lag of the features on 17–22 February, we consider a reasonable estimate of the period to be 44 h in this case, corresponding to approximately $\omega/f = 0.3$. Using this, together with the estimated phase speeds, we can calculate the corresponding wavenumbers, and the frequency–wavenumber pairs are plotted together with the theoretically derived dispersion diagrams in Fig. 11. Apparently, the agreement is quite good between the modeled and analytically derived dispersion curves. However, it must be stressed that for the high phase speed found along the wide shelf south of Lofoten, the signal may well be a coastal Kelvin wave. In order for this to be a CSW, the wavelength must be as much as 3800 km (Fig. 11), which is more that we would expect for a CSW in this region. Conversely, the wavenumber on the narrow shelf corresponds to a wavelength of approximately 800 km. The observed signal probably contains both type of waves, and it is difficult to distinguish between the two on the wide shelf south of Lofoten. However, the strikingly slower propagation along the shallow shelf along Lofoten cannot be explained by a coastal Kelvin wave, but it does fit nicely with the CSW theory.

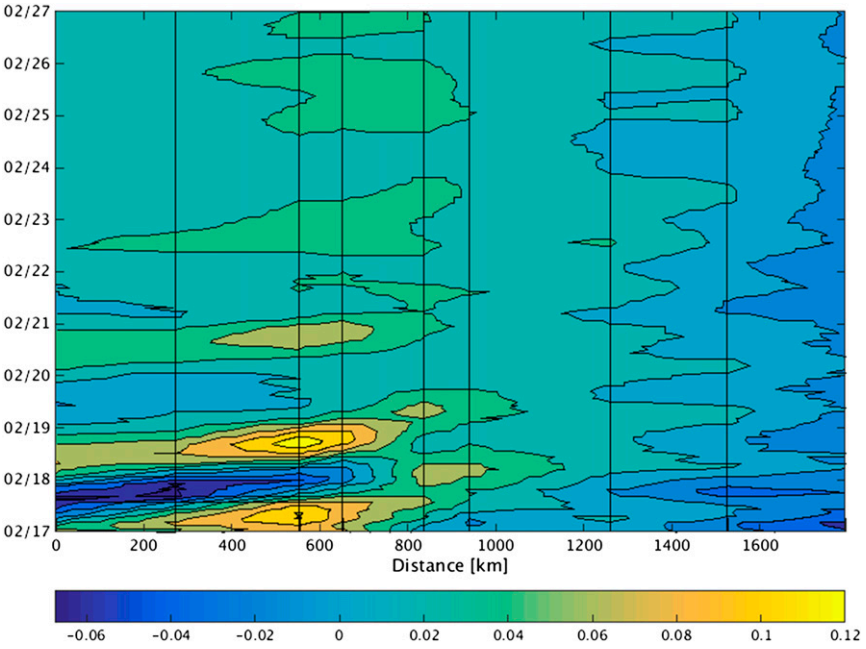

FIG. 10. Hovmöller plots of the SSA from the nine points shown in Fig. 2 for the idealized case of an isolated storm event. Note that the times for February on the *y* axis correspond to times after the storm has ceased. The vertical black lines correspond to the points shown in Fig. 2, starting with the southernmost point (left) going northward (to the right).

6. Summary and concluding remarks

In this study, we have derived a theory for the dispersion of freely propagating continental shelf waves (CSWs), valid for arbitrary shelf width. Our calculations allow for a nonzero divergence of the wave motion. The theory has been applied to the propagation of CSWs along the Norwegian west coast, and farther along the escarpment between northern Norway and the Svalbard archipelago (which in terms of the applied theory can be considered an extremely wide continental shelf). This configuration is close to that supporting double Kelvin waves (Longuet-Higgins 1968). The effect of stratification on CSWs in this region has been investigated by idealized model runs (Gjevik 1991; Slørdal et al. 1994). They conclude that the effect on long CSWs is small.

Assuming that the frequency is conserved, a CSW passing Lofoten has to slow down considerably on the narrow shelf, with a correspondingly shorter wavelength. To pass on to the much wider shelf north of Norway, the wavelength has to increase to more than its original value, with a correspondingly higher phase speed.

Calculations of the dispersion relation for the locations at the Norwegian shelf have also been done using the rigid-lid approximation. This approximation turns out to be very good. The only exception is for the very wide inner shelf north of Lofoten. Here the deviation at the peak frequency from the free-surface value is about 8%.

From realistic model runs, we have demonstrated that sea surface signatures of CSWs are difficult to separate from other barotropic waves such as coastal Kelvin waves along the Norwegian coast. However, the model shows that the barotropic signal propagating

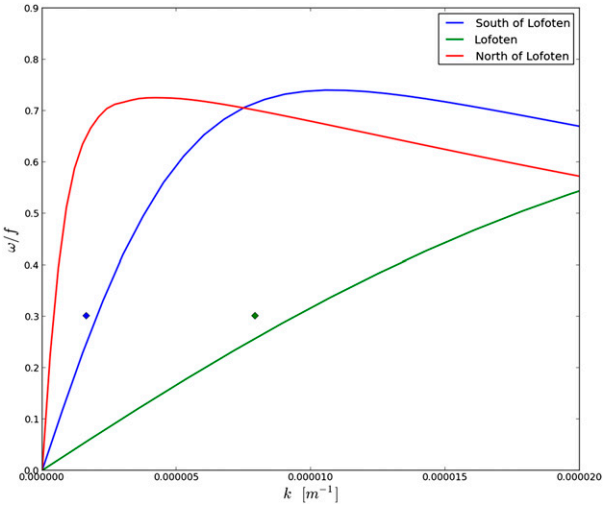

FIG. 11. Zoomed version of Fig. 4 (for the first modes), including frequency–wavenumber pairs from the model run for the wide shelf south of Lofoten (blue diamond) and the narrow shelf west of Lofoten (green diamond).

along the coast slows down significantly when it reaches the narrow shelf outside Lofoten, before speeding up again on the much wider shelf after Lofoten, consistent with the theory for CSWs. Furthermore, when running the model with idealized forcing, that is, an isolated storm event, we find that the sea surface response propagates like a CSW along the narrow part of the shelf. The attenuation of the signal is probably due to the rather strong friction in the numerical model. In addition, there is probably a split in energy between northward propagation along the escarpment and eastward propagation into the Barents Sea.

It must be emphasized that the theoretical results for arbitrary shelf width presuppose an idealized (infinitely long) shelf in the wave propagation direction. The application to real shelves implies that the Wentzel–Kramers–Brillouin (WKB) approximation can be used. For the shelf west of Norway this is somewhat problematic, since, from our analytical results, the change in wavelength over the total length of the shelf is of order one. It is therefore encouraging that the numerical model results for a realistic shelf topography yield frequencies and wavenumbers for the shelf south of Lofoten and outside Lofoten that fit reasonably well with the theory (see, e.g., Fig. 11).

Acknowledgments. Setup of the numerical model was partly done by Yvonne Gusdal during the EU FP7 project ECLISE (Grant 265240). Tide-gauge data from Norwegian Coastal Stations are kindly delivered by Hilde Sande at Norwegian Mapping Authority. Computer resources for the numerical model are delivered in-kind from MET Norway. We gratefully acknowledge financial support from the Research Council of Norway through Grant 20754 (OilWave).

REFERENCES

Allen, J., 1980: Models of wind-driven currents on the continental shelf. *Annu. Rev. Fluid Mech.*, **12**, 389–433, doi:10.1146/annurev.fl.12.010180.002133.

Ball, F., 1967: Edge waves in an ocean of finite depth. *Deep-Sea Res. Oceanogr. Abstr.*, **14**, 79–88, doi:10.1016/0011-7471(67)90030-7.

Björk, G., B. G. Gustafsson, and A. Stigebrandt, 2001: Upper layer circulation of the Nordic seas as inferred from the spatial distribution of heat and freshwater content and potential energy. *Polar Res.*, **20**, 161–168, doi:10.1111/j.1751-8369.2001.tb00052.x.

Brink, K. H., 1991: Coastal-trapped waves and wind-driven currents over the continental shelf. *Annu. Rev. Fluid Mech.*, **23**, 389–412, doi:10.1146/annurev.fl.23.010191.002133.

——, 2006: Coastal-trapped waves with finite bottom friction. *Dyn. Atmos. Oceans*, **41**, 172–190, doi:10.1016/j.dynatmoce.2006.05.001.

——, and D. C. Chapman, 1985: Programs for computing properties of coastal-trapped waves and wind-driven motions over the continental shelf and slope. Tech. rep. WHOI-85-17, Woods Hole Oceanographic Institution, 99 pp., doi:10.1575/1912/5363.

Buchwald, V. T., and J. K. Adams, 1968: The propagation of continental shelf waves. *Proc. Roy. Soc. London*, **305**, 235–250, doi:10.1098/rspa.1968.0115.

Camayo, R., and E. J. Campos, 2006: Application of wavelet transform in the study of coastal trapped waves off the west coast of South America. *Geophys. Res. Lett.*, **33**, L22601, doi:10.1029/2006GL026395.

Chapman, D. C., 1985: Numerical treatment of cross-shelf open boundaries in a barotropic coastal ocean model. *J. Phys. Oceanogr.*, **15**, 1060–1075, doi:10.1175/1520-0485(1985)015<1060:NTOCSO>2.0.CO;2.

Charnock, H., 1955: Wind stress on a water surface. *Quart. J. Roy. Meteor. Soc.*, **81**, 639–640, doi:10.1002/qj.49708135027.

Chen, N., G. Han, J. Yang, and D. Chen, 2014: Hurricane Sandy storm surges observed by Hy-2a satellite altimetry and tide gauges. *J. Geophys. Res. Oceans*, **119**, 4542–4548, doi:10.1002/2013JC009782.

Dee, D. P., and Coauthors, 2011: The ERA-Interim reanalysis: Configuration and performance of the data assimilation system. *Quart. J. Roy. Meteor. Soc.*, **137**, 553–597, doi:10.1002/qj.828.

Echevin, V., A. Albert, M. Lévy, M. Graco, O. Aumont, A. Piétri, and G. Garric, 2014: Intraseasonal variability of nearshore productivity in the Northern Humboldt Current System: The role of coastal trapped waves. *Cont. Shelf Res.*, **73**, 14–30, doi:10.1016/j.csr.2013.11.015.

Flather, R. A., 1976: A tidal model of the northwest European continental shelf. *Mem. Soc. Roy. Sci. Liege*, **10** (6), 141–164.

——, 2000: Existing operational oceanography. *Coast. Eng.*, **41**, 13–40, doi:10.1016/S0378-3839(00)00025-9.

Gascard, J.-C., G. Raisbeck, S. Sequeira, F. Yiou, and K. A. Mork, 2004: The Norwegian Atlantic Current in the Lofoten basin inferred from hydrological and tracer data (^{129}I) and its interaction with the Norwegian Coastal Current. *Geophys. Res. Lett.*, **31**, L01308, doi:10.1029/2003GL018303.

Gill, A. E., 1982: *Atmosphere-Ocean Dynamics.* International Geophysics Series, Vol. 30, Academic Press, 662 pp.

——, and E. H. Schumann, 1974: The generation of long shelf waves by the wind. *J. Phys. Oceanogr.*, **4**, 83–90, doi:10.1175/1520-0485(1974)004<0083:TGOLSW>2.0.CO;2.

Gjevik, B., 1990: Model simulations of tides and shelf waves along the shelves of the Norwegian-Greenland-Barents seas. *Modeling Marine Systems*, Vol. 1, A. M. Davies, Ed., CRC Press, 187–219.

——, 1991: Simulations of shelf sea response due to travelling storms. *Cont. Shelf Res.*, **11**, 139–166, doi:10.1016/0278-4343(91)90059-F.

——, 2000: Summary and assessment of the NDP Metocean project. Project Rep. to the Norwegian Deepwater Project, 53 pp.

——, 2002: Unstable and neutrally stable modes in barotropic and baroclinic shelf slope currents. Matematisk institutt preprint series: Mechanics and applied mathematics, Paper 27810, 18 pp. [Available online at http://urn.nb.no/URN:NBN:no-27810.]

Haidvogel, D., and Coauthors, 2008: Ocean forecasting in terrain-following coordinates: Formulation and skill assessment of the regional ocean modeling system. *J. Comput. Phys.*, **227** (7), 3595–3624, doi:10.1016/j.jcp.2007.06.016.

Hamon, B., 1962: The spectrums of mean sea level at Sydney, Coff's Harbour, and Lord Howe Island. *J. Geophys. Res.*, **67**, 5147–5155, doi:10.1029/JZ067i013p05147.

Huthnance, J. M., 1975: On trapped waves over a continental shelf. *J. Fluid Mech.*, **69**, 689–704, doi:10.1017/S0022112075001632.

——, 1978: On coastal trapped waves: Analysis and numerical calculation by inverse iteration. *J. Phys. Oceanogr.*, **8**, 74–92, doi:10.1175/1520-0485(1978)008<0074:OCTWAA>2.0.CO;2.

——, 1987: Effects of longshore shelf variations on barotropic continental shelf waves, slope currents and ocean modes. *Prog. Oceanogr.*, **19**, 177–220, doi:10.1016/0079-6611(87)90007-3.

——, 1995: Circulation, exchange and water masses at the ocean margin: the role of physical processes at the shelf edge. *Prog. Oceanogr.*, **35**, 353–431, doi:10.1016/0079-6611(95)80003-C.

Kaoullas, G., and E. Johnson, 2010: Fast accurate computation of shelf waves for arbitrary depth profiles. *Cont. Shelf Res.*, **30**, 833–836, doi:10.1016/j.csr.2009.12.010.

Longuet-Higgins, M., 1965: Some dynamical aspects of ocean currents. *Quart. J. Roy. Meteor. Soc.*, **91**, 425–451, doi:10.1002/qj.49709139005.

——, 1968: Double kelvin waves with continuous depth profiles. *J. Fluid Mech.*, **34**, 49–80, doi:10.1017/S002211206800176X.

Marchesiello, P., J. C. McWilliams, and A. Shchepetkin, 2001: Open boundary conditions for long-term integration of regional oceanic models. *Ocean Modell.*, **3**, 1–20, doi:10.1016/S1463-5003(00)00013-5.

Martinsen, E., B. Gjevik, and L. P. Røed, 1979: A numerical model for long barotropic waves and storm surges along the western coast of Norway. *J. Phys. Oceanogr.*, **9**, 1126–1138, doi:10.1175/1520-0485(1979)009<1126:ANMFLB>2.0.CO;2.

Middleton, J. F., and J. A. Bye, 2007: A review of the shelf-slope circulation along Australia's southern shelves: Cape Leeuwin to Portland. *Prog. Oceanogr.*, **75**, 1–41, doi:10.1016/j.pocean.2007.07.001.

Mysak, L. A., 1980: Recent advances in shelf wave dynamics. *Rev. Geophys.*, **18**, 211–241, doi:10.1029/RG018i001p00211.

Pedlosky, J., 1982: *Geophysical Fluid Dynamics*. 1st ed. Springer-Verlag, 636 pp.

Sansón, L. Z., 2012: Simple models of coastal-trapped waves based on the shape of the bottom topography. *J. Phys. Oceanogr.*, **42**, 420–429, doi:10.1175/JPO-D-11-053.1.

Schulz, W. J., Jr., R. P. Mied, and C. M. Snow, 2012: Continental shelf wave propagation in the Mid-Atlantic Bight: A general dispersion relation. *J. Phys. Oceanogr.*, **42**, 558–568, doi:10.1175/JPO-D-11-098.1.

Shchepetkin, A. F., and J. C. McWilliams, 2005: The regional oceanic modeling system (ROMS): A split-explicit, free-surface, topography-following-coordinate oceanic model. *Ocean Modell.*, **9**, 347–404, doi:10.1016/j.ocemod.2004.08.002.

Sheng, J., X. Zhai, and R. J. Greatbatch, 2006: Numerical study of the storm-induced circulation on the Scotian Shelf during Hurricane Juan using a nested-grid ocean model. *Prog. Oceanogr.*, **70**, 233–254, doi:10.1016/j.pocean.2005.07.007.

Slørdal, L. H., E. A. Martinsen, and A. F. Blumberg, 1994: Modeling the response of an idealized coastal ocean to a traveling storm and to flow over bottom topography. *J. Phys. Oceanogr.*, **24**, 1689–1705, doi:10.1175/1520-0485(1994)024<1689:MTROAI>2.0.CO;2.

Smith, R., 1972: Nonlinear kelvin and continental-shelf waves. *J. Fluid Mech.*, **52**, 379–391, doi:10.1017/S002211207200148X.

Thiebaut, S., and R. Vennell, 2010: Observation of a fast continental shelf wave generated by a storm impacting Newfoundland using wavelet and cross-wavelet analyses. *J. Phys. Oceanogr.*, **40**, 417–428, doi:10.1175/2009JPO4204.1.

Weber, J. E. H., and M. Drivdal, 2012: Radiation stress and mean drift in continental shelf waves. *Cont. Shelf Res.*, **35**, 108–116, doi:10.1016/j.csr.2012.01.001.

Webster, I., 1987: Scattering of coastally trapped waves by changes in continental shelf width. *J. Phys. Oceanogr.*, **17**, 928–937, doi:10.1175/1520-0485(1987)017<0928:SOCTWB>2.0.CO;2.

Wilkin, J. L., 1988: Scattering of coastal-trapped waves by irregularities in coastline and topography. Ph.D. thesis, Massachusetts Institute of Technology and Woods Hole Oceanographic Institution, 120 pp., doi:10.1575/1912/4956.

——, and D. C. Chapman, 1987: Scattering of continental shelf waves at a discontinuity in shelf width. *J. Phys. Oceanogr.*, **17**, 713–724, doi:10.1175/1520-0485(1987)017<0713:SOCSWA>2.0.CO;2.

Woodham, R., G. B. Brassington, R. Robertson, and O. Alves, 2013: Propagation characteristics of coastally trapped waves on the Australian continental shelf. *J. Geophys. Res. Oceans*, **118**, 4461–4473, doi:10.1002/jgrc.20317.

Yankovsky, A. E., and D. C. Chapman, 1995: Generation of mesoscale flows over the shelf and slope by shelf wave scattering in the presence of a stable, sheared mean current. *J. Geophys. Res.*, **100**, 6725–6742, doi:10.1029/94JC03339.